PORT SAID ENGINEERING JOURNAL
Faculty of Engineering - Port Said University
Volume 25 No. 2 September 2021 pp. 146 - 154
-Production Engineering and Mechanical Design-

Effect of Crack Orientation and Residual Stress on Stress Intensity Factors of Butt-Welded Steel Joints

E. El Shrief [1], A. El-Megharbel[2], A. El Domiaty[3], H. Abd El-Hafez[4,5]

ABSTRACT

Assessing the structural integrity of a cracked weldment is crucial. Cracks detected during welding inspections must be examined in the context of the structure's mechanical resistance. Generally, fracture mechanics supplies essential tools to determine a fracture criterion for loading conditions. This study explores the effect of residual stress (RS) and cracks orientation on determining the stress intensity factor (K_I) for a welded joint using the extended finite element method. This study comprises a 3D thermo-mechanical finite element (FE) analysis to study the temperature history and the residual stress distribution of a welded joint, and a 3D FE crack model that considers two cases of cracks—longitudinal (case I) and transverse (case II)—to calculate the K_I value at the middle surface of a thin butt joint. K_I is calculated for cracks under applied external and residual stresses. The results demonstrate that the welding residual stress can beneficially or detrimentally affect K_I depending on stress distribution and sign, and indicate the significance of RS and crack orientation on K_I. Simulation results demonstrate that the longitudinal crack in case I has higher K_I values than those in case II for the transverse crack and show good agreement with the analytical results.
Keywords: Welding residual stress; Stress intensity factor; Fracture mechanics; Crack orientation; Stainless steel

1. INTRODUCTION

Welding plays a major role in joining methods owing to its manufacturing efficiency and structural reliability [1]. However, the welding process induces residual stresses and, occasionally, defects such as cracks. These can be detrimental to a structure, contributing to fatigue damage and stress corrosion behavior [2]. The combination of cracks and residual stresses is especially harmful to the structure. To estimate the integrity of a welded joint with respect to residual stress fields, determining their effects on the major parameters of the crack, such as the stress intensity factor (K_I), using linear elastic fracture mechanics (LEFM) [3] is crucial. The extended finite element method (XFEM) has been developed as an extensive numerical technique for examining the crack propagation simulation. In recent years, XFEM has been the subject of considerable research as a powerful numerical procedure for the analysis of cracks [4].

[1]*Production Engineering and Mechanical Design Department, Faculty of Engineering, Port Said University, Port Said, Egypt, email:eman.ahmed@eng.psu.edu.eg Corresponding author*

[2]*Production Engineering and Mechanical Design Department, Faculty of Engineering, Port Said University, Port Said, Egypt, email: aelmegharbel@eng.psu.edu.eg,*

[3]*Mechanical engineering Department, Faculty of Engineering, Suez Canal University, Egypt, Email alyeldomiaty@eng.scu.edu.eg.com*

[4]*Production Engineering and Mechanical Design Department, Faculty of Engineering, Port Said University*

[5]*Department of Mechanical Engineering, College of Engineering, Qassim University, Unaizah, Saudi Arabia Email, abdelhafez1@eng.psu.edu.eg*

Received: 03-10-2020, Accepted 15-02-2021
DOI: 10.21608/PSERJ.2021.44187.1065

Within the framework of thermo-elastic fracture, Duflot investigated the static case of thermo-elastic fracture by XFEM, which considered thermal boundary conditions with different crack faces for 2D and 3D problems [5]. Moreover, Zamani and Eslami [6] implemented XFEM to model the effects of the mechanical load and the thermal shocks on a plate with a stationary crack. Gadallah et al. [7] modelled a 3D plate with a semi-elliptical surface crack. Through-thickness residual stresses were presented across two methods. First, the crack face traction solution was studied with the superposition theory. Second, 2D residual stress analysis results were applied and mapped to a crack FE model. K_I results were first compared with the Newman–Raju solution and were then expanded to welded models by comparing the mechanical loading and the actual residual stress distribution.

Qiang et al. [8] investigated through-thickness welding residual stress in thick butt-welded Q345qD steel plate through finite element analysis (FEA) and experimental studies. FEA and the weight function method were used to calculate K_I results for semi-elliptical surface cracks in a butt weld and the effect of the weld residual stress on K_I was observed. Ferro et al. [9] studied the influence of multi-pass welding on the residual stress field near the weld toe for a butt-welded joint. Furthermore, the influence of welding RS on the fatigue and fracture properties of a welded steel bridge was examined using analytical and FEA methods.

Generally, XFEM is performed on a thermo-elastic fracture model of the welding thermal effect to study the temperature, stress, and fracture parameters (K_I) for a center-cracked structure subject to a moving heating source. In this study, the stress intensity factor K_I was computed numerically using the XFEM method for through cracks located in the center of the butt joint. The

effects of the welding residual stresses and the crack orientation on K_I values are studied; the results are compared with the theoretical solution achieved by the weight function method.

2. THE PRINCIPLE OF XFEM

The XFEM is an addition to the traditional finite element method and is based on the concept of the unit partition technique. The modeling of cracked structures is simplified by XFEM because there is no need to modify the mesh to study a crack [10]. Establishing a reasonable refinement mesh around the crack is essential to achieving accurate results when determining. The basis of XFEM is a procedure of displacement field approximation that can model the discontinuity along a crack face and crack tip singularity [4, 10]. In classical FEM, it is difficult to extract the numerical values of displacements through numerical integration. Consequently, XFEM was established to more easily calculate singular problems. Moreover, it accounts for discontinuities in an FE description by increasing the degrees of freedom with special displacement functions that are connected to the elements influenced by the crack. The displacement field for the extended finite element approximation used for crack modeling is defined with the following equation [10, 11]:

$$U_{xfem}(x) = \sum_{i=I} N_i(x)U_i + \sum_{i=J} N_i(X)H(x)a_i + \sum_{i=k}[N_i(X)\sum_{n=1}^{4} F_n(X)b_{in}] \quad (1)$$

where $U_{xfem}(x)$ is the displacement vector, N_i is the nodal shape function, I is the number of conventional nodes in the model, and U_i is the nodal displacement vector for the non-enriched nodes. J represents the number of nodes enriched with the generalized Heaviside function or jump function (X) and k denotes the nodes enriched with the crack-tip function (X). Values a and b are the additional enriched nodal degree of freedom vectors for (X) and $F_n(X)$, respectively.

3. STRESS INTENSITY FACTOR ANALYSIS

The stress intensity factor K_I characterizes the most significant parameter in linear elastic fracture mechanics. According to fracture mechanics theory, K_I is a function of the stress, crack size, shape, and orientation of the crack, and dimensions of the structure. There are a few techniques for estimating K_I, such as the crack tip displacements extrapolation, ASTM geometrical factor, weight function, the J-integral, and the stress extrapolation technique [10, 12]. In this study, the values of K_I are determined using a modified J-integral and the superposition method and compared, as outlined in the following sections.

3.1. Computation of K_I by The j-integral Method

J-integral methods are widely used practices in FE software packages for determining K_I. However, the J-integral is no longer path-independent in the presence of thermal strains. Consequently, the J-integral is not suitable for this analysis because it does not have constant values and it is dependent on the path [3]. In this study, a modified J-integral technique is used to evaluate the K_I values.

When the residual stresses are observed as secondary stresses, they do not contribute to the collapse of the plastic portion of the J-integral; they only contribute to the elastic portion. The effect of the residual stresses can be combined into the J-integral as follows [13]:

$$J = \left[\sqrt{J_{ext}^{el}} + \sqrt{J_{RS}}\right]^2 + J_{ext}^{pl} \quad (2)$$

where J_{ext}^{el} is the linear elastic J (small yielding zone) due to the external load and J_{ext}^{pl} is the fully plastic J due to the external load. Lei [14] suggested a path-independent integral that can be applied to common crack problems with a combination of primary and secondary stresses. The modified J-integral can be written as follows:

$$J = \int_{\Gamma} \left(V\delta_{1i} - \sigma_{ij}\frac{\partial u_j}{\partial x_1}\right) n_i ds + \int_A \left(\sigma_{ij}\frac{\partial \varepsilon_{ij}}{\partial x_1} - \frac{V}{\partial x_1}\right) \quad (3)$$

where V is the strain energy, $V = \int_0^{\varepsilon_{ij}} \sigma_{ij}(d\varepsilon_{ij}^{el} + d\varepsilon_{ij}^{pl})$ and σ_{ij}, $\varepsilon_{ij}^{el}, \varepsilon_{ij}^{pl}$, and u_j represent the stress, elastic strain, plastic strain, and displacement, respectively [14]. δ_{1i} is the Kronecker delta. For the initial strain problems, the total strain can be expressed as follows:

$$\varepsilon_{ij} = \varepsilon_{ij}^{el} + \varepsilon_{ij}^{pl} + \varepsilon_{ij}^{0} \quad (4)$$

where $\varepsilon_{ij}^{el}, \varepsilon_{ij}^{pl}, \text{and } \varepsilon_{ij}^{0}$ represent the elastic, plastic, and initial strains, respectively. Further, x_1 is the direction of the crack, ni is the unit vector normal to Γ, ds is the path length on the contour Γ, and A is the area surrounded by Γ [14]. In the LEFM approach [4], the J-integral is used to analyze the stress intensity factor K_I as follows:

$$K_I = \sqrt{JE} \quad (5)$$

3.2. Calculation of K_I by The Superposition Method

When there are residual stresses in the materials, in LEFM, the effective $K_{I_{(eff)}}$ is equivalent to the sum of K_{ext} due to the external load and K_{res} due to the residual stresses, according to the superposition method [3] as follows:

$$K_{I_{(eff)}} = K_{ext} + K_{res} \quad (6)$$

K_{ext} for the through-cracked finite plate can be calculated by the following relation [15]:

$$K_{ext} = \sigma_{app}\sqrt{\pi a}\sqrt{\sec\frac{\pi a}{W}} \quad (7)$$

where σ_{app} is the applied stress, W is the width of the welded plate, and a is the half-crack length.

Tada et al. [15] used Green's function to estimate the stress intensity factor K_I due to the longitudinal residual stress (σ_{xx}).

$$\sigma_{xx} = \sigma_0[1 - \left(\frac{z}{c}\right)^2]\, e^{(\frac{-z^2}{2c^2})^2} \quad (8)$$

where σ_0 is the maximum tensile stress in the welding region, 2c is the average plastic tension zone around the weld, and z is the lateral distance from the weld line [16]. Once the residual stress distribution is stated by Eq. (8), K_{res} is expressed as follows:

$$K_{res} = \frac{2}{\sqrt{\pi a}} \int_0^a \frac{\sigma_{xx}\, dx}{\sqrt{1-(\frac{z}{a})^2}} \qquad (9)$$

4. NUMERICAL ANALYSIS OF WELDED JOINT

Model and Material Definition

A model of a butt-welded joint of two 304 stainless steel plates (200 mm ×150 mm × 2 mm), Figure 1, was created in ABAQUS 6.14-1. The temperature-dependent material properties of 304 stainless steel reproduced from [17] are essential for the simulation of welding. The arc welding is carried out along the long length with a constant welding speed of 2.5 mm/s; the convection heat transfer is 60×10^{-6} (W/mm^2 .C), the welding current is 200 A, and voltage is 25V.

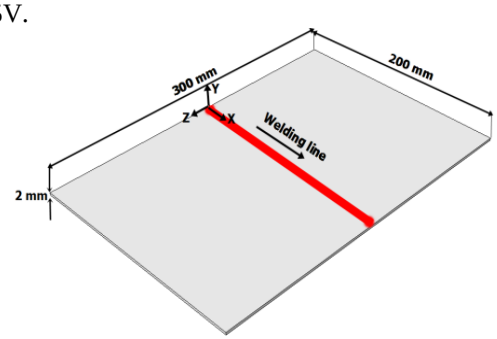

Figure 1: Dimensions of the geometrical model.

4.1. Sequential Thermo-Mechanical Analysis

The sequentially coupled thermo-mechanical model is obtained using the grouping of the ABAQUS code and DFLUX subroutine via FORTRAN to estimate the temperature distribution and the residual stresses in welded joints.

The thermo-mechanical analysis is carried out through thermal analysis followed by mechanical analysis, which uses the thermal analysis results as a load. Figure 2 illustrates the indirect finite element thermo-mechanical method.

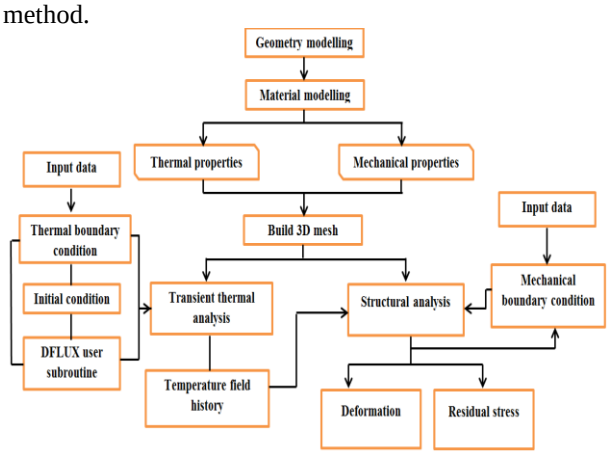

Figure 2: Flow chart for 3D thermo-mechanical finite element analysis.

The 3D-FE meshed model of a butt-welded plate is illustrated in Figure 3. A half model of the welded plate is simulated with symmetric boundary conditions along the weld centreline. The mesh design assumed that there is no separation between the plates and that the welding is performed without the filler metal. A refined mesh was implemented around the weld region to simulate the heat source model. Regular linear diffusive heat transfer elements were used (DC3D8 in ABAQUS for 3D) in the thermal analysis. During the mechanical analysis, fully integrated linear elements, with additional incompatible bending modes (C3D8I in ABAQUS for 3D), occurred.

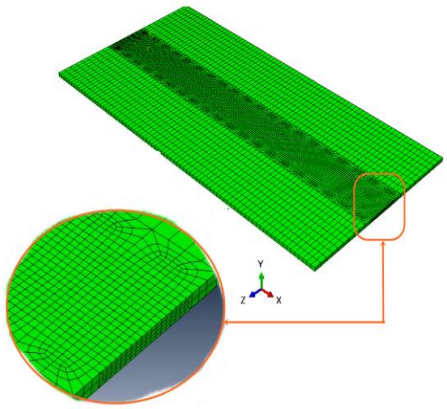

Figure 3: Mesh details for the finite element model of a butt-welded plate.

4.1.1. Thermal Analysis

Thermal analysis was performed on the transient thermal field induced in the material by welding. Figure 4 illustrates Rosenthal's moving heat source model and the fusion zone along the welding line [17], which is used to study the behaviour of the temperature distribution. The temperature distribution is expressed as follows:

$$T(\xi, y, z) - T_0 = \frac{q}{2\pi K\sqrt{\xi^2+y^2+z^2}}\, e^{-\frac{s}{2\alpha}(\xi+\sqrt{\xi^2+y^2+z^2})} \qquad (10)$$

where T_0 is the initial temperature, q is the heat rate value (J/s), K is the thermal conductivity (W/mm.°C), s is the welding speed (mm/s), α is the thermal diffusivity (mm^2/s), and ξ denotes the moving coordinates expressed as ($\xi = x - s\,\tau$), where τ is the time when the welding occurs.

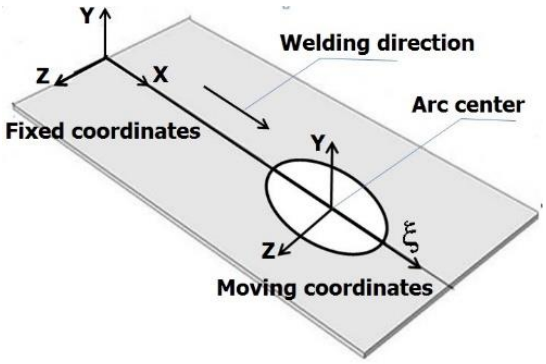

Figure 4: Rosenthal's moving heat source model scheme.

The welding heat from a moving heat source is considered as an alternative form of a circular surface

heat source (Gaussian distributed heat source model). The heat power flux q is expressed as follows [17]:

$$q = \frac{\eta\, Q_p}{\pi b^2}\, e^{\frac{-3z^2}{b^2}}\, e^{\frac{-3\xi^2}{b^2}} \qquad (11)$$

where η is the thermal efficiency of the welding process, Q_p is the absolute power of the source (J/mm), Q_p= (v* I)/s where v is the arc voltage, I is the welding current, s is the welding speed, and b is the radius of the heat source. In the welding simulation, to determine the temperature fields, thermal analysis is performed using thermal boundary conditions based on the heat transfer theory, in which heat transfer occurs from the heat source to the weldment via conduction. The fundamental governing equation of the heat transfer becomes [18]:

$$\frac{\partial}{\partial x}\left(K(T)\frac{\partial T}{\partial x}\right)+\frac{\partial}{\partial y}\left(K(T)\frac{\partial T}{\partial y}\right)+\frac{\partial}{\partial z}\left(K(T)\frac{\partial T}{\partial z}\right)+Q = \rho(T)c_p(T)\frac{\partial T}{\partial t} \qquad (12)$$

where K is the thermal conductivity, T is the temperature, Q is the welding heat, c_p is the specific heat, t is the time and ρ is the density. After the heat source passes, the weldment is cooled to room temperature by convection. Convection heat is defined as:

$$q_{con} = h(T - T_c) \qquad (13)$$

where q_{con} is the convection heat, h is the convection heat transfer coefficient (W /mm^2 C), T is the weldment temperature, and T_c is the surrounding temperature.

4.1.2. Mechanical Analysis

The mechanical analysis was performed based on the values of the thermal–elastic-plastic equations. Through the welding process, the joint is strained as a result of the thermal effect. Hence, the total strain (ε_{total}) estimated from the mechanical analysis is based on the assumption that total strain on the joint is the sum of the thermal strain (ε^{th}), elastic strain (ε^{el}), and plastic strain (ε^{pl}) [2, 19].

$$\varepsilon_{total} = \varepsilon^{th} + \varepsilon^{el} + \varepsilon^{pl} \qquad (14)$$

The stress and the strain can be associated using generalized Hook's law [20, 21]. The stress-strain relation can be written as:

$$[d\sigma] = D^{ep}[d\varepsilon] - [c^{th}]dT \qquad (15)$$

where $[d\sigma]$ is the stress increment, $[D^{ep}]$ is the elastic and plastic stiffness matrices, $[c^{th}]$ is the thermal stiffness matrix, $[d\varepsilon]$ is the strain increment, and dT is the temperature increment.

The symmetric boundary conditions are set on the symmetry plane to reduce computer configuration and time. Moreover, the mechanical boundary conditions must be forced to prevent rigid body motion if the plate is modelled with no constraints (e.g. clamps are omitted) as shown in Figure 5. In the present work, two bottom points in the welding centreline are constrained in the y and x directions. However, tolerant deformations occur only because of the thermal cycle.

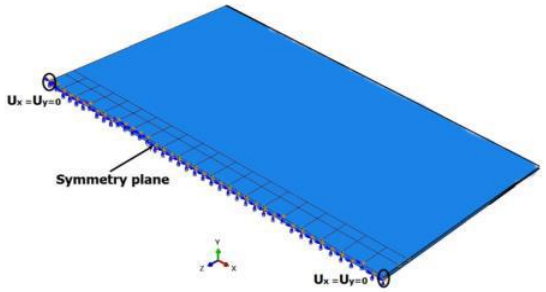

Figure 5: Mechanical boundary conditions

5. NUMERICAL ANALYSIS OF THE FRACTURE MODEL

Weld cracks and residual stresses have serious and unsafe effects on the welding joint. To study the crack orientation behavior in the residual stress fields, determining the fracture parameters of the crack, such as the stress intensity factors K_I, in the presence of welding residual stresses is essential.

5.1. Crack Modelling

The weld residual stress distributions at every nodal point are calculated by a 3D thermo-mechanical nonlinear FEA of the un-cracked plate presented in Figure 1. Newly cracked plates were modelled under two cases to observe the effect of the residual stress on the weld cracks as shown in Figure 6. Case (I) represents a butt-joint with a central through-thickness crack 2a (perpendicular to the welding line). This is introduced in the selected location of the FEM computational domain in Figure 6(a). Case (II) represents a butt-joint with a longitudinal through-thickness crack 2a (in the direction of the welding line) as displayed in Figure 6(b). The analysis indicates that the residual stress distribution is mapped from the 3D thermo-mechanical FE model to the 3D FE crack model as the initial condition, as presented in Figure 7.

Boundary Conditions

Figure 8 depicts the boundary conditions for the two cases of cracked plates. The external uniform mechanical stress σ_{xx} (ext) = 200 MPa is applied in welding direction for case (I); however, σ_{zz} (ext) = 200 MPa is perpendicular to the welding direction for case (II). The fixed displacements for two directions (Uy = Uz = 0) are applied on the load surface. All degrees of freedom along the reverse surface are fixed in both cases (Ux = Uy = Uz = 0), (URx= URy = URz = 0).

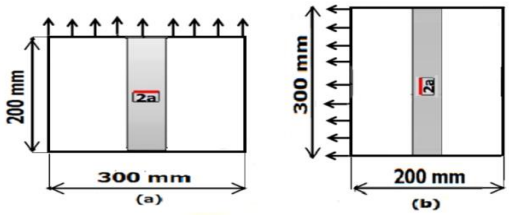

Figure 6: Loading and dimensions for the cracked joints, where 2a represents the crack: a) case (I): transverse crack, and b) case (II): longitudinal crack.

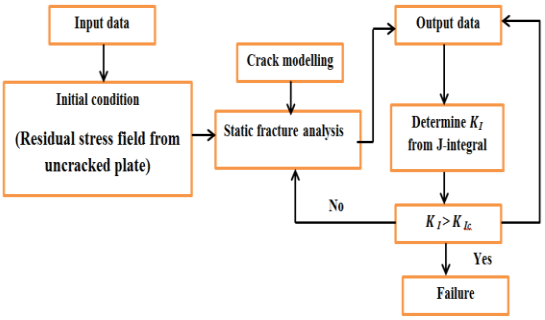

Figure 7: Flow chart for the 3D crack analysis.

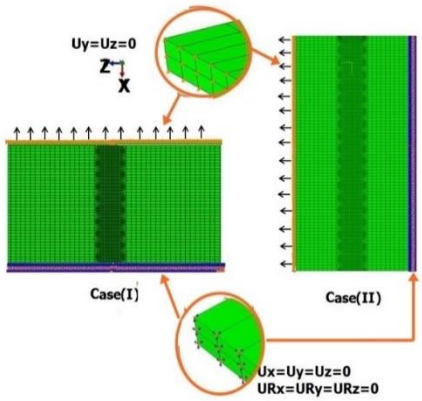

Figure 8: Boundary conditions and loading for the through-cracked thin plate.

The stress intensity factor (K_I) was calculated for the butt joint, particularly for different cracks (longitudinal and transverse). For comparative purposes, five different half-crack lengths, 2, 4, 8, 12, 22 mm, were modelled. For each case, three load models were established: the residual stress, the applied tensile stress, and a combination of them. The analysis cases for the butt joint model are illustrated in Table 1

Table 1: Conditions of the K_I analysis for different model

Number	Crack case	Applied load
1	Case (I)	Applied tensile load
2	Case (I)	Residual stress
3	Case (I)	Residual stress+ tensile load
4	Case (II)	Applied tensile load
5	Case (II)	Residual stress
6	Case (II)	Residual stress+ tensile load

6. RESULTS AND DISCUSSIONS

6.1. Welding Temperature History

The elastic stress–strain relation is not linear when the material is heated beyond its melting temperature. Figure 9 shows the temperature distribution in the plate during the heating process. The recorded temperature after 1.4 s was approximately 1820 °C (Figure 8(a)). Subsequently, the temperature increased by approximately 5% to reach 1927 °C 30 s after the start of the heating process (Figure 8(b)). This result is attributed to conduction heat transfer, in which the advancing zone is affected by the heat source. The temperature remained at a quasi-steady state for the remainder of the welding process, except at the plane end, where it increased by approximately 9% owing to a lack of conduction heat transfer (Figure 8(d)).

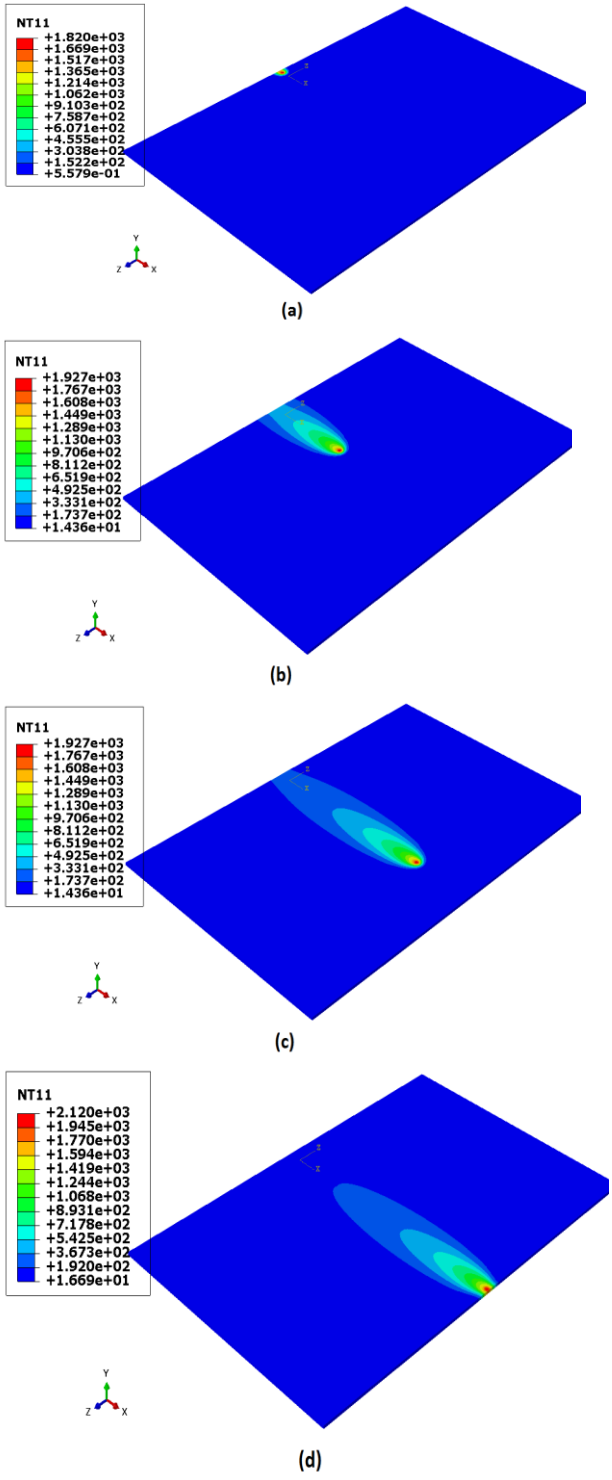

Figure 9: Temperature contour of the plane without cracks in the heating process: (a) t = 1.4 s, (b) t = 30 s, (c) t = 60 s, (d) 79.4 s; t denotes the time after the heating process is started.

The cooling time was estimated after the completion of the welding process (i.e. in 80 s) and the removal of the heat source. The decrease in the temperature variance through the plane plate is related to heat convection (Figure 10(a)). After approximately 1500 s, the temperature gradually decreased to room temperature (Figure 10(b)).

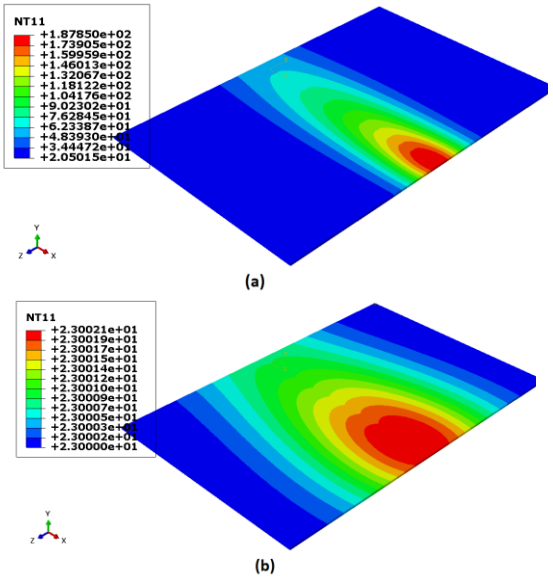

Figure 10: Temperature contour of the plane during the cooling process: (a) t =119.5 s and (b) t = 1500 s; t denotes the time after the completion of the welding process.

For the case presented in Figure 8(c), the temperature histories of the four paths (1–4) were tracked from the starting edge of the plate, where the heat source was positioned at 150 mm from the plate edge after 60 s. Figure 10 plots the predicted temperatures. The four paths represent the temperature in the x–z plane. These results were obtained in two dimensions, as the third dimension was exceedingly small with respect to the other dimensions. The starting edge was still hot (≈200 ˚C) for all paths when the heat source was positioned at 150 mm from the start of the heating process.

Furthermore, the temperature in the x direction along the EF path, 60 s after the start of the welding process, is shown in Figure 11. The results indicate that the temperature decreased when the distance from the heat source increased significantly, owing to convection and conduction heat transfer. Approximately 10 mm from the heat source, the plate had a comparatively lower temperature (≈85 °C).

6.2. Residual Stress Analysis Results

The difference between the thermal expansion and the contraction of the weld and base material is the main parameter that is affected by the welding residual stress. As demonstrated in Figure 13, the simulated longitudinal residual stresses (σxx) on the middle surface are approximately 280 MPa and are located in the welding and the heat affected zones (HAZs). As the distance from the welding centre line increases, the longitudinal tensile stresses gradually decrease, and they are balanced by the compressive stress that is induced in the plates.

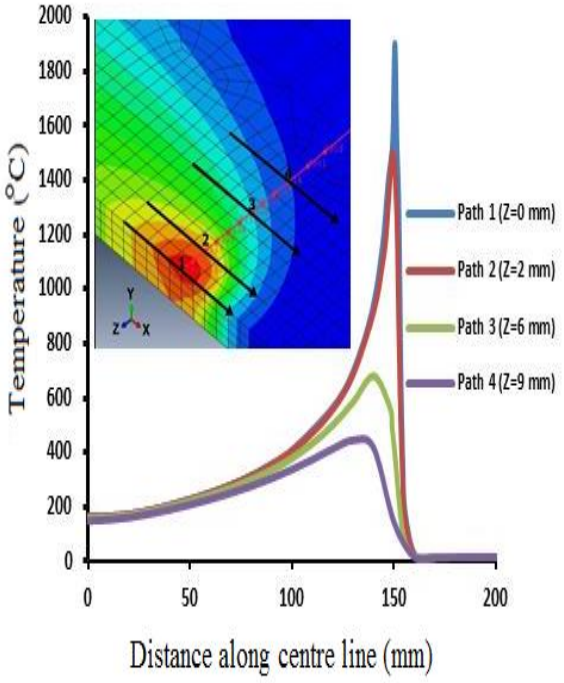

Figure 11: Temperature history in the x–z plane.

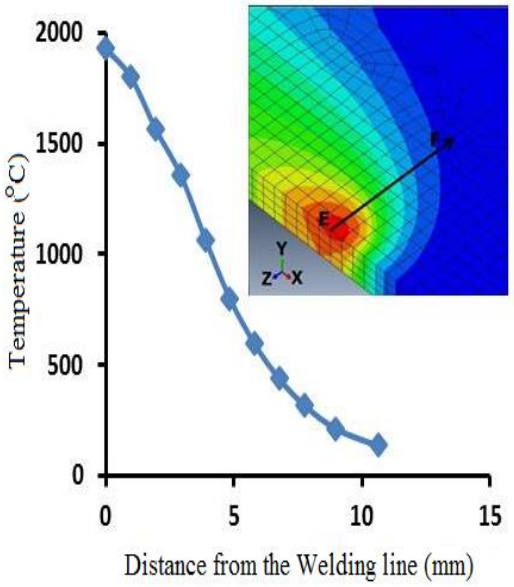

Figure 12: Temperature distribution along the EF path.

Figure 14 depicts the transverse residual stress σ_{zz} on the middle surface in which the variation of the stress is small in the x-direction except for the edges of the plate. Consequently, from the fracture mechanics viewpoint, only stresses in the central part of the plate, where the transverse stress is considered to be constant, are of importance. The through-thickness stress, $\sigma_{yy,}$ is omitted because it exhibits minute variation when compared to the other stresses.

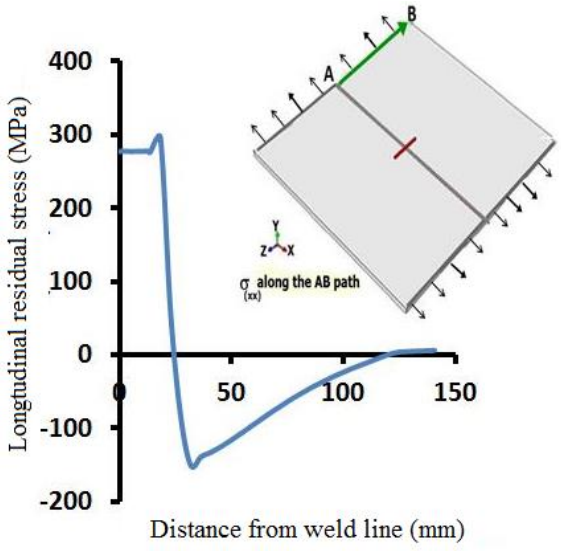

Figure 13: Longitudinal residual stress σ_{xx} (MPa) along the AB path.

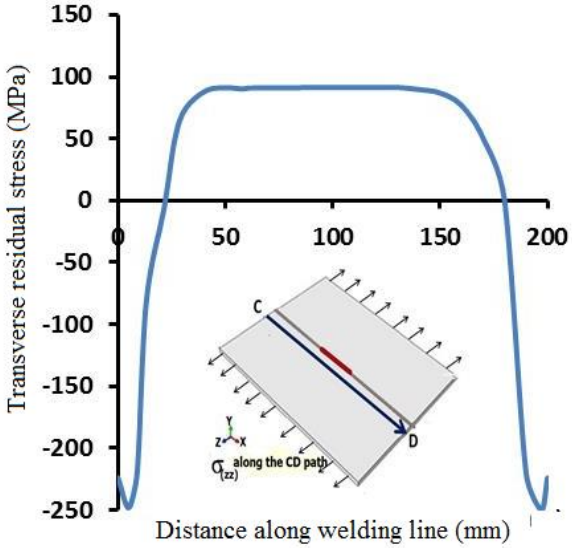

Figure 14: Transverse residual stress σ_{zz} (MPa) along the CD path.

Stress Intensity Factor (K_I) Results

To check the validity of the results, the K_I values for the butt-weld model for the different crack sizes for the two cases were calculated by XFEM in ABAQUS using a modified J-integral method; these results were compared with the analytical solution based on the weight function (superposition method) as given in Eq. (6).

6.2.1. Comparison of the K_I Value under External Stress Only

Figure 15 shows the K_I variation for an external constant stress only. It can be observed from results that the values of K_I increases with the increase in crack length (a/w) in cases (I) and (II).

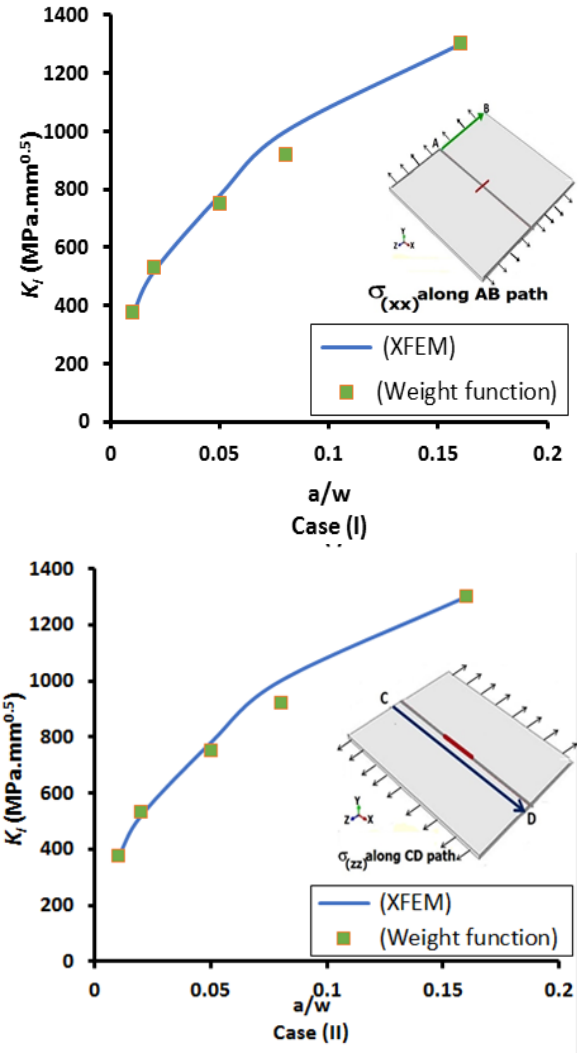

Figure 15: The values of K_I subject to external stress only.

6.2.2. Comparison of the K_I Value Under a Combination of Residual and Applied Stress

The relationship between the K_I values and the crack length for cases (I) and (II) for applying RS only and a combined residual and applied stress is illustrated in Figure 16 and Figure 17 respectively. The different variations in the amplitude of the K_I values of the transverse crack in Figure 16 are due to the nonlinearity of the stress distribution of the longitudinal RS (σ_{xx}). The tensile σ_{xx} causes a substantial increase in K_I for a small crack length. This is located in the fusion zone, or the HAZ; subsequently, the values of K_I decrease in the far-field with an increasing crack length because the crack tip enters the compressive RS region. The variation of σ_{zz} in thin plates has insignificant fluctuation values except when close to the plates' edges. Thus, from the fracture mechanics point of view, only the stresses in the central part of the plate are of interest. Therefore, the stress values may be considered constant, along the welding line in path CD. The effect of σ_{zz} on K_I is small since the transverse residual stress is rather low as depicted in

Figure 17. There is also a good agreement between the analytical and numerical results.

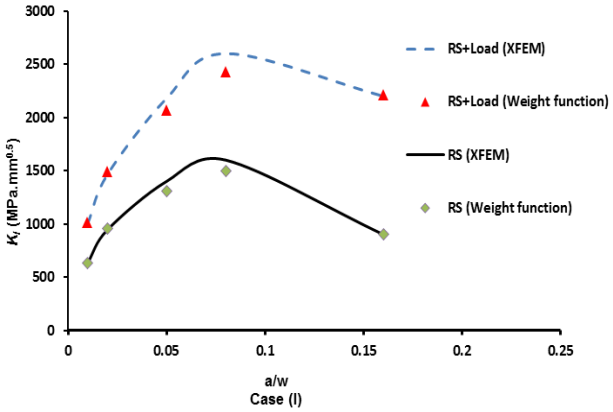

Figure 16: The values of K_I subject to RS and combination of RS and external stress in Case (I).

Table 2 summarises the calculated K_I values at a = 2 mm. The K_I results exhibit a variance of 0.25% and 3.2% between the analytical and XFEM results for cases (I) and (II), respectively. The results indicate that the XFEM results are in good agreement with the analytical solution. XFEM models that use the modified J-integral method are thus valid for determining a constant value for the stress intensity factor K_I in the presence of residual stress.

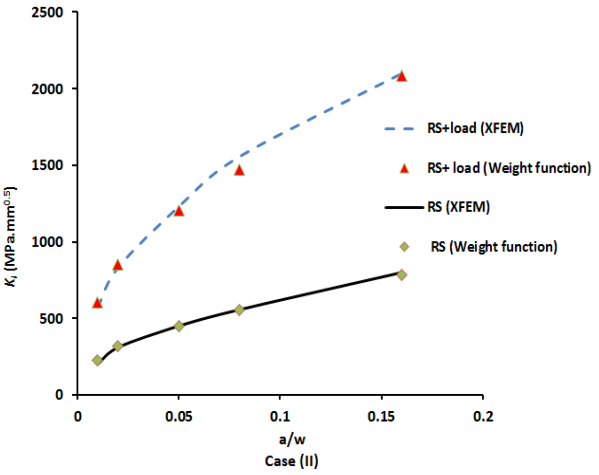

Figure 17: The values of K_I subject to RS and combination of RS and external stress in Case (II).

Table 2: The error of K_I values between XFEM and weight function at crack length a = 2 mm.

K_I (MPa.mm$^{0.5}$), a = 2 mm		
	Case (I) **Load +RS**	Case (II) **Load +RS**
Weight function	1008.15	601.25
XFEM	1005.6	581.6
Difference %	0.25%	3.2%

7. CONCLUSION

This study explores the effects of welding residual stresses and the crack orientation on K_I values for through cracks by performing XFEM; the results were then compared with the analytical solution. Based on the achieved results in this study, the following conclusions can be drawn:

- In the presence of the RS field, the stress intensity factors parameter has the path-dependent plastic thermal strain and does not produce constant results. Therefore, the J-integral method is not suitable for evaluating K_I due to the weld thermal RS.
- The modified J-integral method considers the effects of the RS and it provides a path independent parameter. This parameter is qualified to study crack behaviour under any type of stress, especially the thermal RS.
- The RS and crack orientation have a noticeable effect on K_I. It can be concluded that the effect of the welding RS on K_I is either beneficial or detrimental, depending on the stress sign and the distribution. Also, σ_{zz} is almost constant and it has the same sign along the welding line except along the edges of the joint, where K_I has an insignificant variation for the longitudinal crack.
- σ_{xx} attends the tension-compression stress behavior, which produces a higher K_I in the tensile region and K_I increases with increasing crack length. However, when the crack tip enters the compressive stress, the compressive stress offsets the contribution of the external load and it decreasesK_I.
- Since σ_{zz} is small in comparison to σ_{xx}, K_I is larger in case (I) than in case (II).

The achievement of this method can be extended, such as this work permits to study the redistribution of residual stress during the crack growth in a butt-welded joint. In addition, the fatigue crack growth can be detected in cracked joints under constant and variable loads using the XFEM method.

Credit Authorship Contribution Statement:
E. El Shrief: Software, Resources, Investigation, Data Curation, &Writing. **A. El-Megharbel:** Validation, Writing, supervision, Review & Editing. **A. El Domiaty**: Conceptualization, Investigation, Resources, supervision. **H. Abd El-Hafez**: Validation, Formal analysis, Writing, Supervision – Review & Editing.

Declaration of competing interest
The authors declare that there is no conflict of interest regarding the publication of this paper.

References

[1] J.-H. Lee, B.-S. Jang, H.-J. Kim, S. H. Shim, and S. W. Im, "The effect of weld residual stress on fracture toughness at the intersection of two welding lines of offshore tubular structure," *Marine Structures*, vol. 71, p. 102708, 2020.

[2] D. W. J. Tanner, "Life assessment of welded INCONEL 718 at high tempertature.," Ph.D. Thesis, The University of Nottingham, 2009.

[3] R. Seifi, "Effect of Residual Stress on Fracture Parameters of through Cracks` in Welded Plates," *Procedia Engineering*, vol. 10, pp. 1895-1900, 2011.

[4] S. El Fakkoussi, H. Moustabchir, A. Elkhalfi, and C. Pruncu, "Computation of the stress intensity factor KI for external longitudinal semi-elliptic cracks in the pipelines by FEM and XFEM methods," *International Journal on Interactive Design Manufacturing*, vol. 13, no. 2, pp. 545-555, 2019.

[5] M. Duflot, "The extended finite element method in thermoelastic fracture mechanics," *International Journal for Numerical Methods in Engineering*, vol. 74, no. 5, pp. 827-847, 2008.

[6] A. Zamani, M. R. Eslami, and Structures, "Implementation of the extended finite element method for dynamic thermoelastic fracture initiation," *International journal of solids structures*, vol. 47, no. 10, pp. 1392-1404, 2010.

[7] R. Gadallah, N. Osawa, and S. Tanaka, "Evaluation of stress intensity factor for a surface cracked butt welded joint based on real welding residual stress," *Ocean Engineering*, vol. 138, pp. 123-139, 2017.

[8] B. Qiang, Y. Li, C. Yao, and X. Wang, "Through-thickness welding residual stress and its effect on stress intensity factors for semi-elliptical surface cracks in a butt-welded steel plate," *Engineering Fracture Mechanics*, vol. 193, pp. 17-31, 2018.

[9] P. Ferro, F. Berto, and N. James, "Asymptotic residual stress distribution induced by multipass welding processes," *International Journal of Fatigue*, vol. 101, pp. 421-429, 2017.

[10] G. Qian, V. F. González-Albuixech, M. Niffenegger, and E. J. E. F. M. Giner, "Comparison of KI calculation methods," vol. 156, pp. 52-67, 2016.

[11] A. R. Khoei, *Extended finite element method: theory and applications*, First ed. Wiley, 2014.

[12] R. Bao, X. Zhang, and N. A. Yahaya, "Evaluating stress intensity factors due to weld residual stresses by the weight function and finite element methods," *Engineering Fracture Mechanics*, vol. 77, no. 13, pp. 2550-2566, 2010.

[13] X. Ren, "Effect of welding residual stress on fracture," Ph.D. Thesis, Norwegian University of Science and Technolgy, 2010.

[14] Y. Lei, "J-integral evaluation for cases involving non-proportional stressing," *Engineering Fracture Mechanics*, vol. 72, no. 4, pp. 577-596, 2005.

[15] H. Tada, P. C. Paris, and G. R. Irwin, "The stress analysis of cracks," *Handbook, Del Research Corporation*, vol. 34, 1973.

[16] G. Wu, C. Aird, and M. Pavier, "The effect of residual stress on a centre-cracked plate under uniaxial loading," *International Journal of Fracture* vol. 219, no. 1, pp. 101-121, 2019.

[17] D. Darmadi, J. Norrish, and A. K. Tieu, "Analytic and finite element solutions for temperature profiles in welding using varied heat source models," 2011.

[18] A. S. Ahmad, Y. Wu, H. Gong, and L. Nie, "Finite element prediction of residual stress and deformation induced by double-pass TIG welding of Al 2219 plate," *Materials* vol. 12, no. 14, p. 2251, 2019.

[19] A. El Megharbel, G. El Nasser, and A. El Domiaty, "Bending of tube and section made of strain-hardening materials," *Journal of Materials Processing Technology*, vol. 203, no. 1-3, pp. 372-380, 2008.

[20] A. S. Ahmad, Y. Wu, H. Gong, and L. Liu, "Determination of the effect of cold working compression on residual stress reduction in quenched aluminum alloy 2219 block," *SV-JME*, vol. 65, pp. 311-318, 2019.

[21] E. El-shrief, M. Saber, A. Nassef, and M. Shaker, "Numerical Simulation to Study the Influence of Welding Sequence on Distortion and Residual Stresses of Butt-Welded Plates," *Port-Said Engineering Research Journal.*, vol. 20, no. 1, pp. 118-126, 2016.